robotics

MDPI

Article

Design, Implementation, and Kinematics of a Twisting Robot Continuum Arm Inspired by Human Forearm Movements

Alaa Al-Ibadi [1,2,*], Khalid A. Abbas [1], Mohammed Al-Atwani [1] and Hassanin Al-Fahaam [1]

[1] Computer Engineering Department, University of Basrah, Basrah 64001, Iraq; khalid.abbas@uobasrah.edu.iq (K.A.A.); mohammed.kade@uobasrah.edu.iq (M.A.-A.); hassanin.husein@uobasrah.edu.iq (H.A.-F.)
[2] School of Computing, Science and Engineering, University of Salford, Salford M5 4WT, UK
* Correspondence: alaa.abdulhassan@uobasrah.edu.iq or a.f.a.al-ibadi@edu.salford.ac.uk

Abstract: In this article, a soft robot arm that has the ability to twist in two directions is designed. This continuum arm is inspired by the twisting movements of the human upper limb. In this novel continuum arm, two contractor pneumatic muscle actuators (PMA) are used in parallel, and a self-bending contraction actuator (SBCA) is laid between them to establish the twisting movement. The proposed soft robot arm has additional features, such as the ability to contract and bend in multiple directions. The kinematics for the proposed arm is presented to describe the position of the distal end centre according to the dimensions and positions of the actuators and the bending angle of the SBCA in different pressurized conditions. Then, the rotation behaviour is controlled by a high precision controller system.

Keywords: soft robotics; pneumatic muscle actuators (PMA); twisting; kinematics; human forearm

Citation: Al-Ibadi, A.; Abbas, K.A.; Al-Atwani, M.; Al-Fahaam, H. Design, Implementation, and Kinematics of a Twisting Robot Continuum Arm Inspired by Human Forearm Movements. *Robotics* **2022**, *11*, 55. https://doi.org/10.3390/robotics11030055

Academic Editor: Po-Yen Chen

Received: 7 April 2022
Accepted: 19 April 2022
Published: 22 April 2022

1. Introduction

Biological inspiration leads to an extensive number of inventions around the world. A rigid robot is just one example of an invention that has benefited us, either in industrial applications or in our social lives. However, using these machines in close proximity to humans has dramatically increased during the last decade, which has led to an increased risk of injury. Soft robots are a good alternative to rigid robots when it comes to health and safety due to their impressive advantages.

The softness of the material that is typically used to build soft robotics provides the term 'soft' and is normally used to cover the entire robot body without any rigid joints. One widely-used soft actuator is the pneumatic muscle actuator (PMA), which offers various benefits, such as being lightweight, having the variety and flexibility to be built into different structures [1–5], having high degrees of freedom (DoF) [6–8], safe to individuals and can be implemented by various dimensions [2,5].

However, the PMA behaves at high nonlinearity [4,5,9–11], such as hysteresis and time dependence. The inner rubber tube elasticity properties and the braided mesh [2,4] These concerts make the modelling and controlling of the soft systems more complicated [1,12,13].

Despite the general similarity in soft PMAs, each design can show a unique performance, one of these prototypes is the OctArm by [14], which shows adaptability, flexibility and efficient performance. Nevertheless, it is not easy to build and control as it is constructed from many actuators. This design shows mechanical difficulties. The Air-Octor soft arm in [15] is noticeably less complicated to build and control because the body of the arm is a single soft PMA and it is actuated by tendons. Though, the friction of the cables decreases its performance, which produces unpredicted changes in cable binding and moves the trunk in indefinite performance. A soft arm of three sections of six extensor PMA in the first two sections and three extensor actuators in the Section 3 is proposed

by [16]. Each actuator can be activated separately, while the control of airflow shows multiple degrees of freedom.

Another prototype is given by [17], this continuum arm is constructed by a single extension PMA and three cables to control its distal end. This model curves in an arc, However, the authors give no information about grasping the produced force.

A continuum arm of four contraction actuators, which can contract and bend in different directions is built by [18]. A similar effect is given when using extensor PMAs to build an extension soft arm to provide the ability for extension and bending [19]. Another design has been presented by the authors for a bending arm that uses a single self-bending contraction actuator (SBCA) [20]. On the other hand, a twisting copper wire is inserted into a soft body to provide a bending behaviour and twisting behaviour by using the wire itself [21]. A similar technique is used by [22] to establish a bending behaviour for a finger. A robot arm by 3D printable origami has been used by [23] and it is driven by tendons. A prototype of a variable stiffness twisted rubber and it is driven by a stepper motor is presented by [24] present a variable stiffness twisted rubber and it is driven by a stepper motor.

Numerous prototypes have been presented in the area of grasping techniques by using the pneumatic actuators [25–29]. Various continuum robots have been designed and built recently [30,31] however, designing simple, reliable, and high-performance soft robots remain the major challenge. This robot needs to be easy to model and control [17,32]. More challenges are shown when the robot is required to perform several applications. To achieve the design goal, the designer needs to consider every single link and performance by modelling, simulation, and control.

According to its design, the pneumatic air muscle shows linear behaviour such as contraction and extension. An innovative design of contraction PMA is presented by [33] which provides a mechanical design that allows the muscle slides on a shaft and shows 30% more tensile force than the traditional contraction PMA Furthermore, the modified actuators offer bending and diameter reduction behaviour [20,34,35] Though, the air muscle does not have the capability to twist itself.

On the other hand, the rigid mechanical systems show a different point of view. While they provide a good precision performance, the rigidity, low force to weight ratio, is less safe for humans and a high probability of risk of injury [36]. Elongation and deformation of the rigid material due to the strain represent one of the rigid robot drawbacks that need to test and solve [37]. Companies are developing manufacturing methods in addition to the material that is used for production to enhance the Overall Equipment Efficiency (OEE) [38]. Variable stiffness actuators are developed by [39] by using a magnetic torsional spring. Other research has been done to develop such types of actuators to provide less stiffness and more flexibility behaviour for rigid actuators [40,41].

This article presents the basic performances and anatomy of the human upper limb. The inspiration of the twisting performance of the individual forearm has been used to propose a continuum arm of two contraction air muscles and single bending PMA that rotates and bends in numerous directions as an additional feature.

The rest of the article is organised as follows: Section 2 gives the biological anatomy of the human forearm with the principle of twisting behaviour. The design of the robot's soft arm is described in Section 3. While the kinematics of the proposed soft arm is illustrated in Section 4. Experiments are done to validate the kinematics and prove the novelty and efficiency of the proposed arm, in Section 5. Section 6 provides a control system to adjust the twisting angle.

2. The Rotation of the Human Forearm

A pair of two long bones of the human forearm; the ulna and the radius lie in parallel between the elbow and wrist joints [42,43]. The two bones are acting mutually to provide the twisting performance for a human forearm. The ulna has no rotation joint, and it is

considered a fixed bone, while the radius rotates longitudinally about its shaft from the elbow and in semi-circular rotation from the wrist joint.

Twisting toward a clockwise direction is called pronation and the opposite rotation is called supination. The diagonal intersection between radius and ulna is occurring during the pronation as shown in Figure 1. A small fibrous connects the two bones at halfway between the wrist and the elbow and it is studied by academics as an extra joint [44]. The twisting behaviour of the two bones is illustrated in Figure 2. The bones are also linked by an interosseous layer to enlarge the region of the muscular connection along with maintaining a specific correlation between the radius and the ulna.

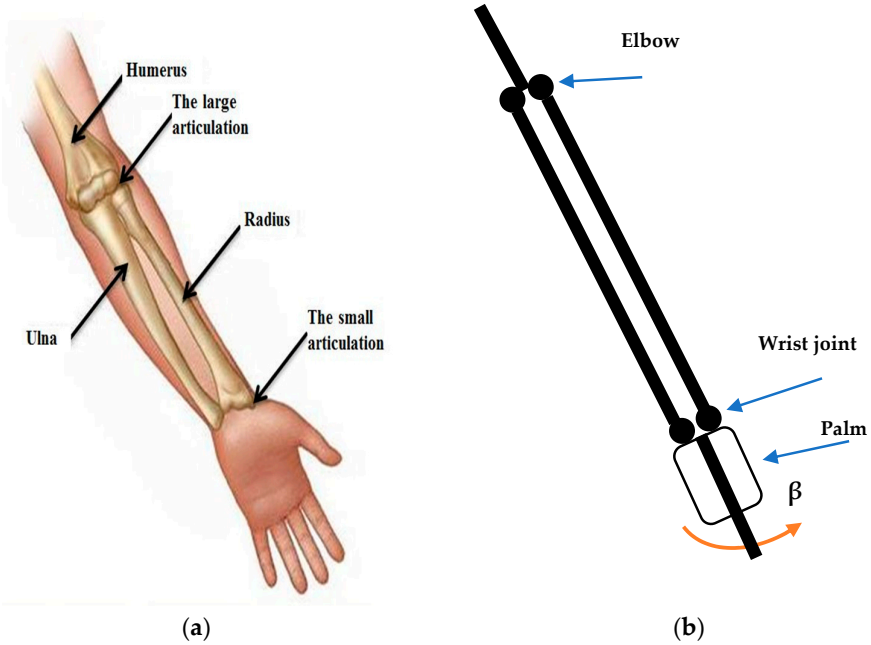

Figure 1. The rotating joints and the bones of the human forearm. (**a**) The biological concepts. (**b**) The schematic configuration.

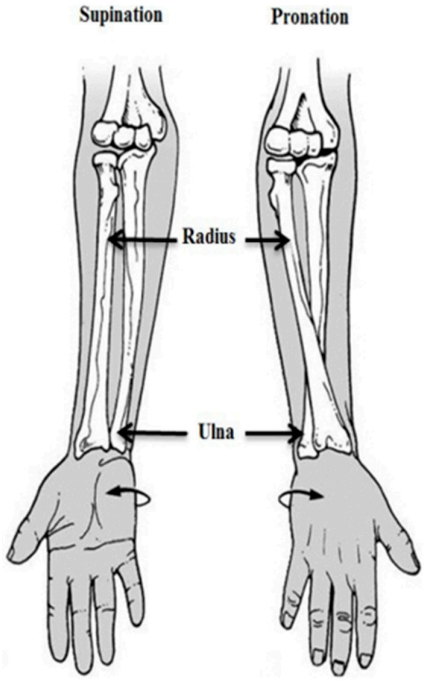

Figure 2. The clockwise and anticlockwise movements.

3. The Design of a Twisting Soft Robot Arm

The human arm-twisting behaviour due to an elbow joint that is described in the previous section has inspired us to design a soft robot arm that can be twisted. The structure of the proposed arm is given in Figure 3. A self-bending contraction actuator (SBCA) is implemented to establish the proposed soft arm's rotating behaviour. The bending actuator is constructed by adding a reinforcement flexible rod of 20 cm long, 0.6 cm width, and 0.2 cm thickness to the 20 cm contraction PMA. The rod is sewn to the braided sleeve to prevent the contraction from that side, as shown in Figure 3a.

When the actuator is pressurised, the addition of the reinforcing rod means that one side of the muscle will be prevented from contracting and remains at its maximum length. This difference in contraction on the two sides of the actuator results in the actuator bending. Further details of the operation of the SBCA can be found in [20].

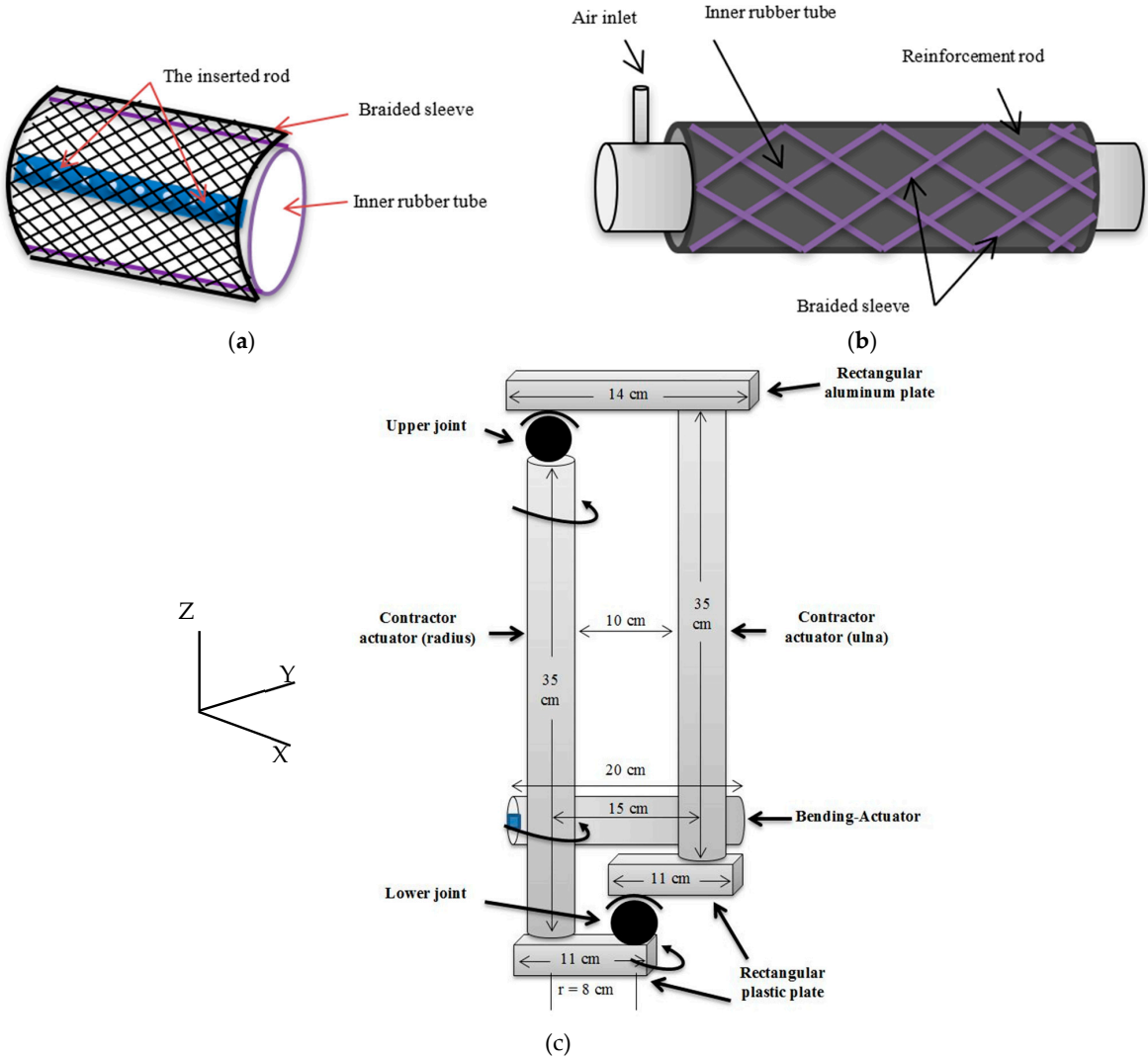

Figure 3. The proposed rotating arm. (**a**) The structure of SBCA design. (**b**) The structure of the contraction PMA. (**c**) The full structure of the proposed arm.

Two contraction actuators of 37 cm in length are used in parallel and one SBCA actuator of 20 cm is positioned between them to establish the twisting. The contraction actuators are made similarly by using a 42 cm inner rubber tube and 42 cm braided mesh and two solid ends of 2.5 cm each. After construction, the unpressurised length is 37 cm (see Figure 3b). Like the ulna bone of the person's forearm, the right contraction PMA is fixed at the elbow and wrist joints as shown in Figure 3c. the other air muscle is laid in

parallel but has been connected to the encoder from the top and the rotating joint from the bottom to twist along its upright axis from the upper, and over the right actuator from the base. This operation behaves similar to the radius of a human arm. To test the twisting angle of the proposed continuum arm, air pressure is applied via the solenoid valve on the SBCA, and the twisting angle is observed by the encoder. The experiment gives that pressurising both contraction actuators simultaneously at any value shows no effect on the twisting angle. The range of the rotating angle is 0° to 91°. As a result, the supination behaviour is occurring in a pressurised condition and the pronation occurs during the venting process.

4. The Kinematics Models of the Twisting Soft Robot Arm

The key behaviour of the proposed soft robot continuum arm is the ability to twist anticlockwise and return clockwise by about 91°, while the human elbow produces about 70° in both directions [45]. However, unlike the human arm, where the radius and ulna are rigid, in this system, they are both formed from flexible actuators, which can be adjusted in length. This means that, in addition to the supination-pronation motion, the arm can also bend as the relative lengths of the radius and ulna are adjusted. The proposed continuum arm provides a wide range of movements according to the quantity of air pressure in every one of the three muscles. These movements represent extra characteristics of the suggested robot arm. Pressurising both contraction actuators at a similar amount leads to shortness of the continuum arm. The maximum safe work pressure is 500 kPa and the maximum contraction ratio for both contraction PMAs is 30% (11 cm). While applied different air pressure on the contraction actuators shows bending behaviour in the right or left direction, the arm bends toward the actuator of high pressure. The SBCA provides the rotation behaviour and shows multi-degree of freedom (DoF) movements with a combination of different air pressure in the contraction PMAs.

The position and orientation for the centre of the free end change under the impact of the different pressures in the three actuators. Figure 4 shows the proposed soft robot arm under different pressurising conditions.

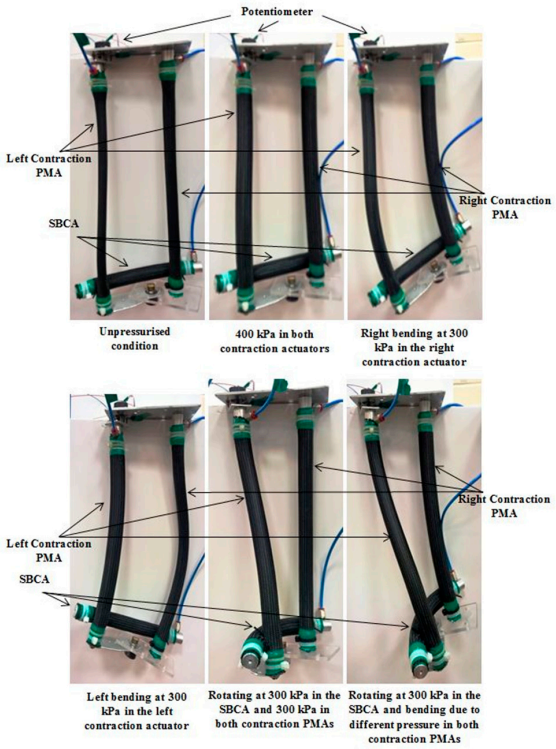

Figure 4. Movement examples of the proposed rotating arm.

To analyse the position and the orientation of the centre point of the distal end, the kinematics for the proposed arm is discussed from three views: *Y-Z*, *X-Y* and *X-Z* planes.

Figure 5a shows the front view of the proposed arm in non-pressurised conditions. Where the length of the left and right contraction actuators at no pressure is defined as L_{01} and L_{02} respectively, r_1 is the length that lay between the left contraction PMA and the centre of the soft arm, and r_2 is the distance between the right contraction PMA and the rotating centre. L_1 and L_2 are lengths under pressurised conditions. Figure 5b–d illustrates the *Y-Z*, *X-Y* and *X-Z* views respectively, at pressurised conditions of the SBCA.

l_1 and l_2 are the linear fronts and side view of L_1 and L_2 respectively, λ_1 is the resultant side distance between the initial point of the first contraction actuator at relaxed conditions of the SBCA and the new location of the first contraction air muscle at pressurised conditions of the SBCA, γ is the deviation angle of the left contraction PMA due to the bending of the SBCA, r_1 and r_2 are the length between the spinning centre and the centre of the contraction air muscles, and β represents the bending position of the bending actuator. The contraction ratio ε of the contraction actuators is defined as:

$$\varepsilon = \frac{L_0 - L}{L_0}, \tag{1}$$

Assuming both contraction actuators are identical, then:

$$L_{01} = L_{02} = L_0 \tag{2}$$

From Figure 5b:

$$l_2 = L_2 = L_0(1 - \varepsilon_2) \tag{3}$$

And:

$$l_1 = L_1 \cos\gamma \tag{4}$$

From Figure 5c:

$$\lambda_1 = r_1 - r_1 \cos\beta \tag{5}$$

Then:

$$\gamma = \sin^{-1}\left(\frac{r_1 - r_1 \cos\beta}{L_1}\right) \tag{6}$$

And from Figure 5e:

$$\phi = \cos^{-1}\left(\frac{r_1 \sin\beta}{L_2}\right) \tag{7}$$

ϕ is the angle between the second contraction muscle and the vertical layout at pressurised conditions. Applying air pressure to the contraction actuators causes a bending angle of φ degrees in the direction of the shortest contraction PMA, as illustrated in Figure 6.

$$\varphi = \sin^{-1}\left(\frac{L_2 - L_1 \cos\gamma}{r_1 \cos\beta + r_2}\right) \tag{8}$$

$$\Delta Z = L_0 - (L_2 - r_2 \ \sin\varphi) \tag{9}$$

$$\Delta Y = r_2 - r_2 \cos\varphi \tag{10}$$

ΔZ and ΔY are the displacements in both Z and Y directions. from the set of equations above, it is easy to find the new position and angle of the rotating centre.

The effect of the deformation of the three actuators on the kinematics of the proposed twisting arm can be ignored due to the rotation ability of the arm and the stiffness of the actuators at pressurised conditions.

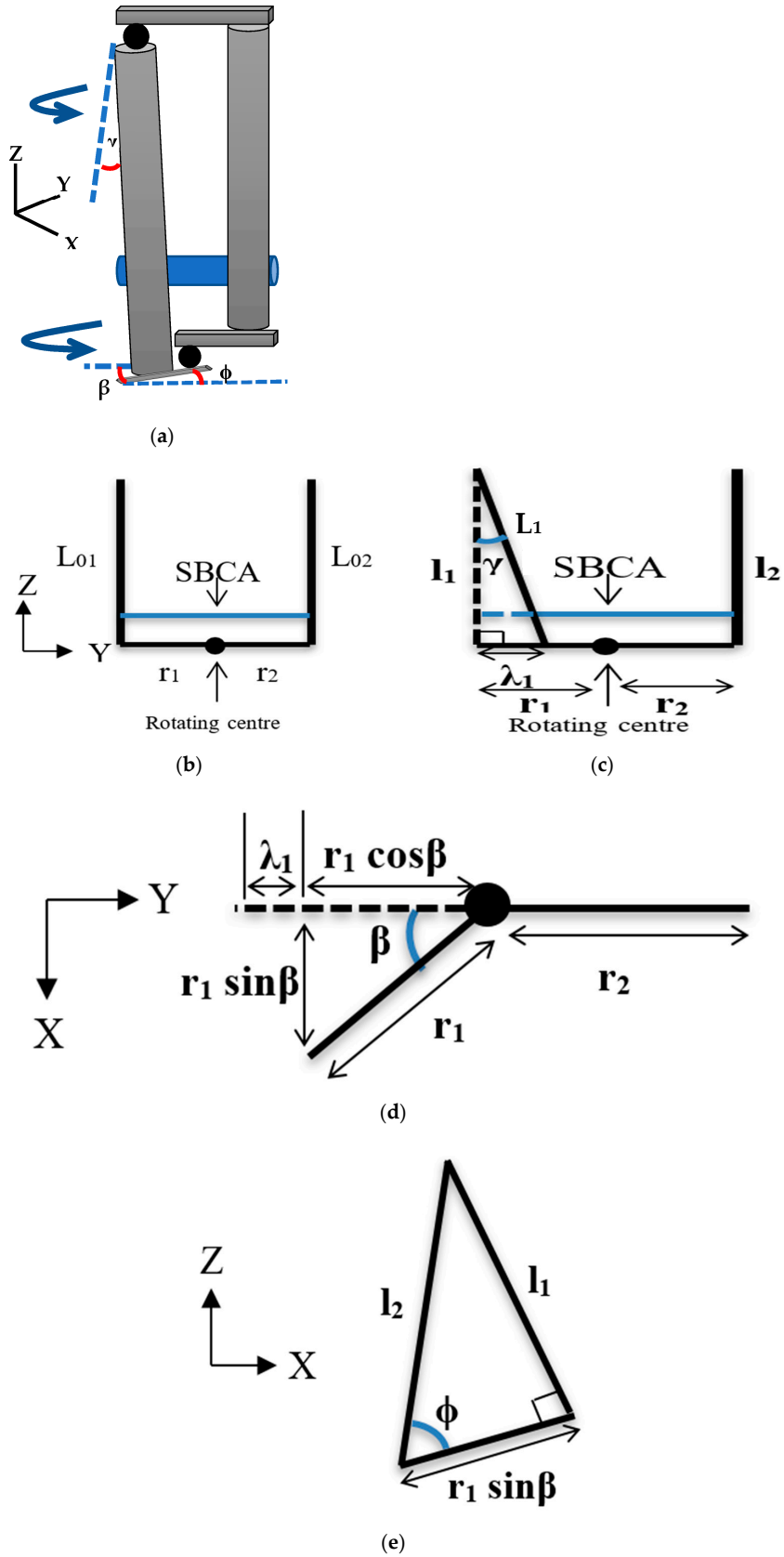

Figure 5. The geometrical analysis of the twisting soft robot arm. (**a**) 3D view of the proposed arm in a twisting condition. (**b**) the front view in relaxed conditions. (**c**) The *Y*-*Z* view under pressurised conditions. (**d**) The *X*-*Y* view under pressurised conditions. (**e**) The *X*-*Z* view under pressurised conditions.

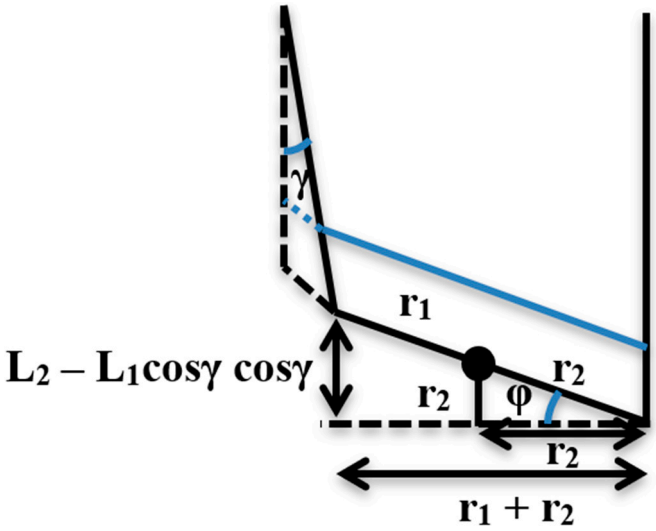

Figure 6. The displacement and the angle of the rotating centre.

5. The Validation and the Experiment Results

In this section, air pressure is applied to the contraction actuators and the SBCA via a (3/3 Matrix) solenoid valve and the pressure in each actuator is measured by an analogue pressure sensor. Since the right contraction PMA is fixed from both sides, the MPU 6050 sensor is fixed to the end of the left contraction PMA to measure the γ angle. The bending angle of the SBCA β is measured by the encoder, which is fixed instead to the upper joint (see Figure 4). Several experiments are done to illustrate the behaviour of the presented twisting soft robot arm. The pressure is increased in the SBCA from 0 to 400 kPa by steps of 50 kPa, and the angle β is measured experimentally. Its data is listed in Table 1. The angles γ, ϕ, and φ are measured experimentally by the MPU sensors and calculated from Equations (6), (7), and (8), respectively.

Table 1. The static characteristics of the SBCA bend angle at different pressure values.

Pressure (kPa)	β (Degree)
0	0
50	24
100	37
150	49
200	59
250	64
300	69
350	74
400	78

Figure 7a–c shows the orientation angles of the rotating centre as a function of the bending angle of the SBCA according to the data in Table 1 at zero air pressure on both contraction actuators. The model results show significant parallels with the experimental data, with small errors, high correlation factors, and similar performances. Despite what the experiment shows when both the contraction actuators are in the relaxed condition, the rotating centre shows a displacement varying in Y and Z directions according to (9) and (10), and are listed in Figure 8.

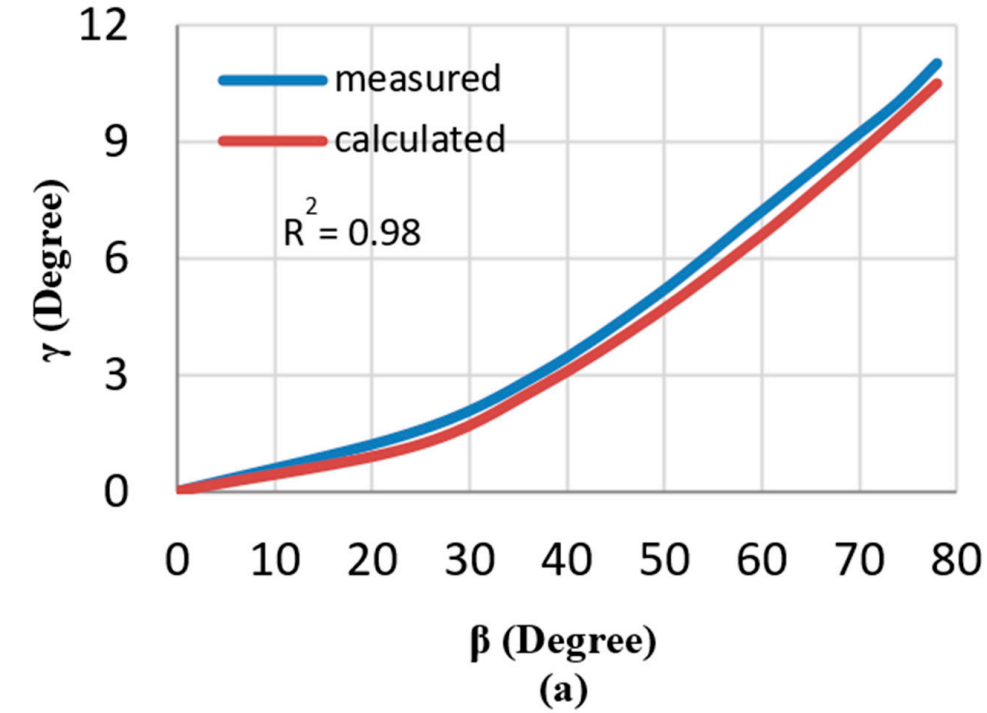

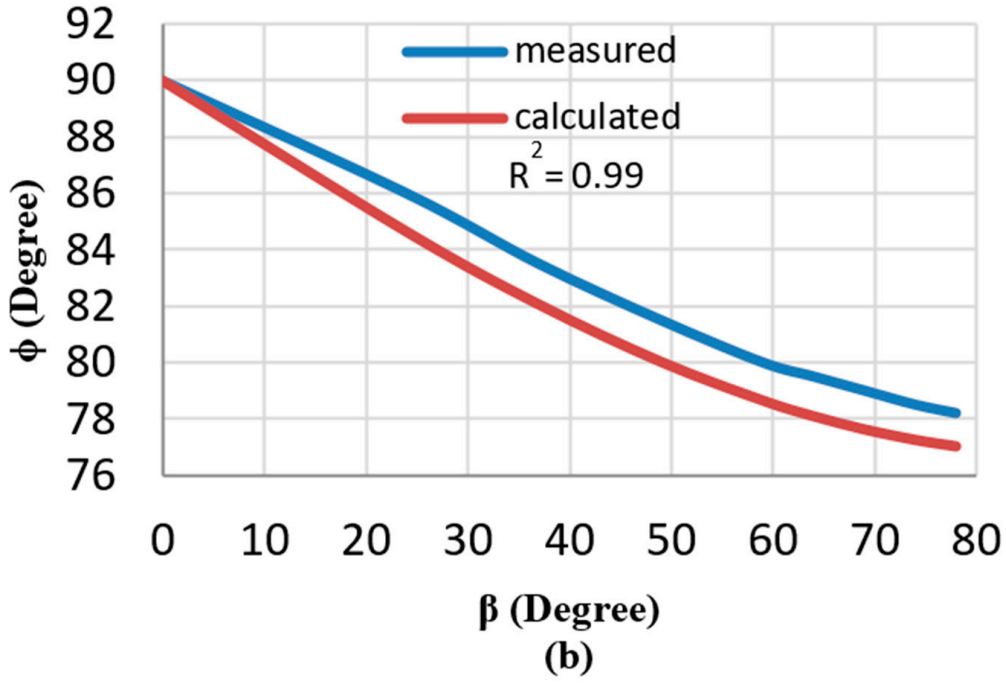

Figure 7. *Cont*.

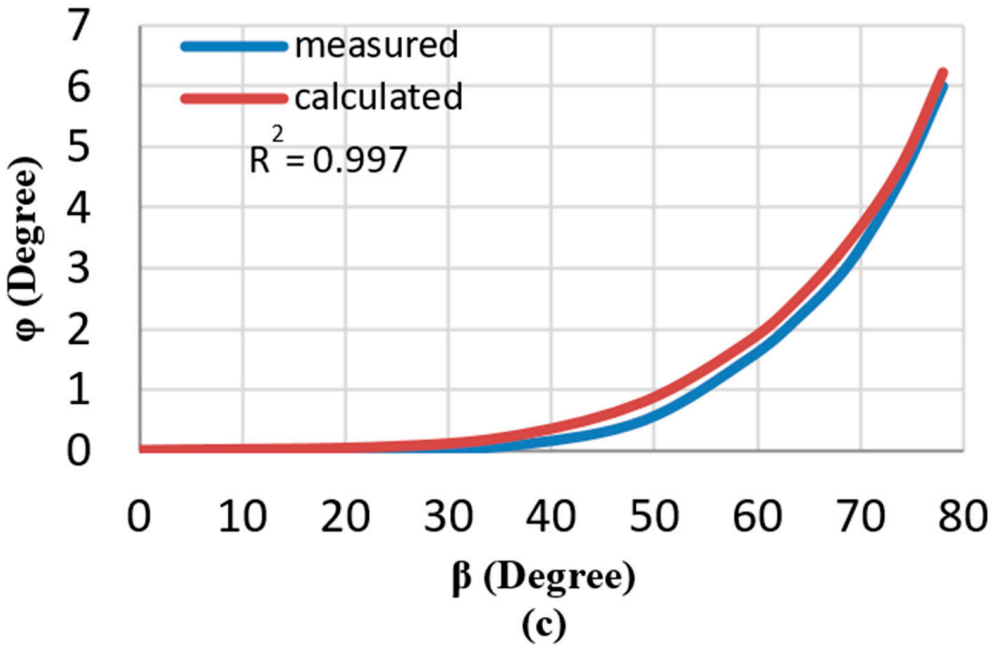

Figure 7. The orientation angles of the rotating centre as a function of β. (**a**) The γ angle. (**b**) The ϕ angle. (**c**) The φ angle.

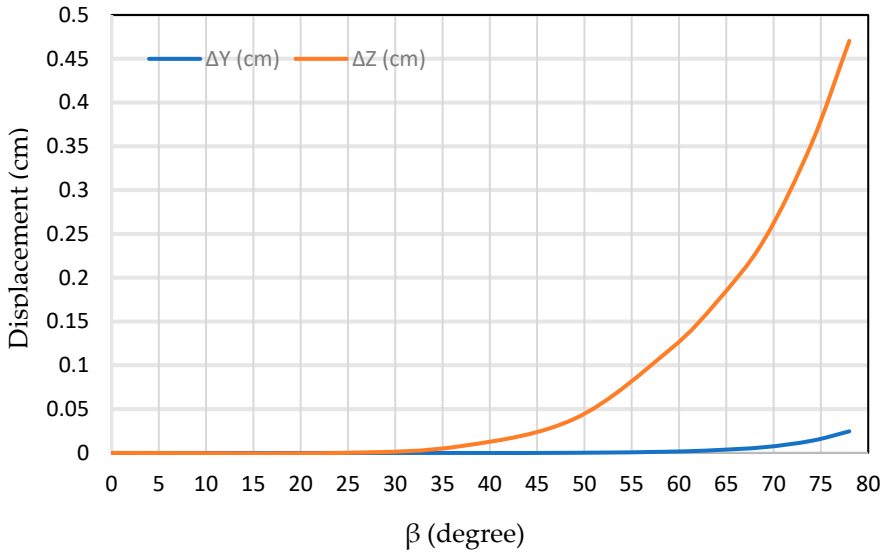

Figure 8. The displacement in Y and Z is due to the change of bending angle.

Applying air pressure to both the contraction PMAs affects all of the parameters (see Equations (6)–(10)), and to demonstrate this impact, air pressure is applied to the left and the right contraction actuators individually. The length variations for both the contraction actuators are listed in Table 2. The length variation between the two contractor actuators is ignored due to the similarity in design and implementation.

Table 2. The length of the contraction actuators at different pressure values.

Pressure (kPa)	L_1 (cm)	L_2 (cm)
0	37	37.05
50	35.3	35.35
100	33	33.05
150	31.5	31.52

Table 2. *Cont.*

Pressure (kPa)	L_1 (cm)	L_2 (cm)
200	30.6	30.65
250	30.1	30.15
300	29.7	29.71
350	29.5	29.54
400	29.2	29.21
450	29.1	29.1
500	29.1	29.1

Three different β values are chosen to demonstrate the effects of L_1 on the presented continuum arm parameters at relaxed conditions for the right contraction actuator. Figure 9a–d illustrates these effects at β equal to (20°, 40°, and 60°) for the calculated and measured data. The angles except for β in these figures have been measured manually three times and the average has been drawn.

The length change of the contraction actuators is defined as:

$$\Delta L_s = L_{0s} - L_s \tag{11}$$

where: s is the number of actuators. Since both the contraction actuators have a similar initial length, then:

$$\Delta L_1 = L_0 - L_1 \tag{12}$$

And

$$\Delta L_2 = L_0 - L_2 \tag{13}$$

Figure 9a shows the behaviour of the γ angle with the raised change in length of the right contraction PMA at three different values of β. This figure illustrates that the increase in ΔL_1 and/or β leads to an increase in γ, and that is a validation of (6) and Figure 7a. Similarly, the increment in φ is due to the increase in ΔL_1 and/or β (see (8) and Figure 7c). The variations of the rotating centre are similarly increased in the Y and Z directions.

The experiment is repeated but at the relaxed pressurising conditions of L_1, and the air pressure is increased in the right contraction actuator according to Table 2. The experiment results are used to calculate ϕ from (7) at three different values of β, then, the angle φ and the changes in the Y and Z positions of the rotating centre are found for (L_1 = 37 cm). The calculating results are found according to (6)–(10) and the measured data is found manually three times, then the average is recorded. Figure 10a–d demonstrates the parameters of the twisting soft arm at different pressurised conditions of the right contraction actuator.

Figure 10a shows that the increase in ΔL_2 and/or β leads to a decrease in the ϕ angle at a fixed length of the left actuator, according to (7). Otherwise, the increment in one or both of ΔL_2 and β leads to a decrease in the value of φ and makes the orientation around X of the rotating centre negative. The comparison between Figures 9b and 10b illustrates that the φ values in a positive direction are more than the values in the negative direction because the rise in β leads to the rise in φ in the positive direction (see Figure 7c). On the other hand, the variation of Y and Z is also raised with the increase in ΔL_2 and/or β. Nevertheless, the variation in Z, due to the change in L_2, is more than the variation due to the change in L_1, because of the effects of the increment of β (see Figure 8).

The experiment results due to the variety in both L_1 and L_2 are validated by comparing the results in Figures 9 and 10 and listed in Table 3 in the terms of coefficient of determination (R^2).

On the other hand, an experiment to observe the load effect on the contraction and twisting angle is done by attaching a load to the end of the proposed arm. The load is varied from zero to 2 kg. As shown in Table 4, the length of the contraction actuators is slightly affected by increasing the attached load, while the variations in twisting angle can be ignored.

In a comparison with the literature, the proposed arm mimics the performances of the human arm at high force. The twisting arm of [21] provides a high twisting angle but at 0.4 N, 2.5 N for the robot arm in [23], and 5 N in [24]. While the contraction PMA provides about 400 N [46]

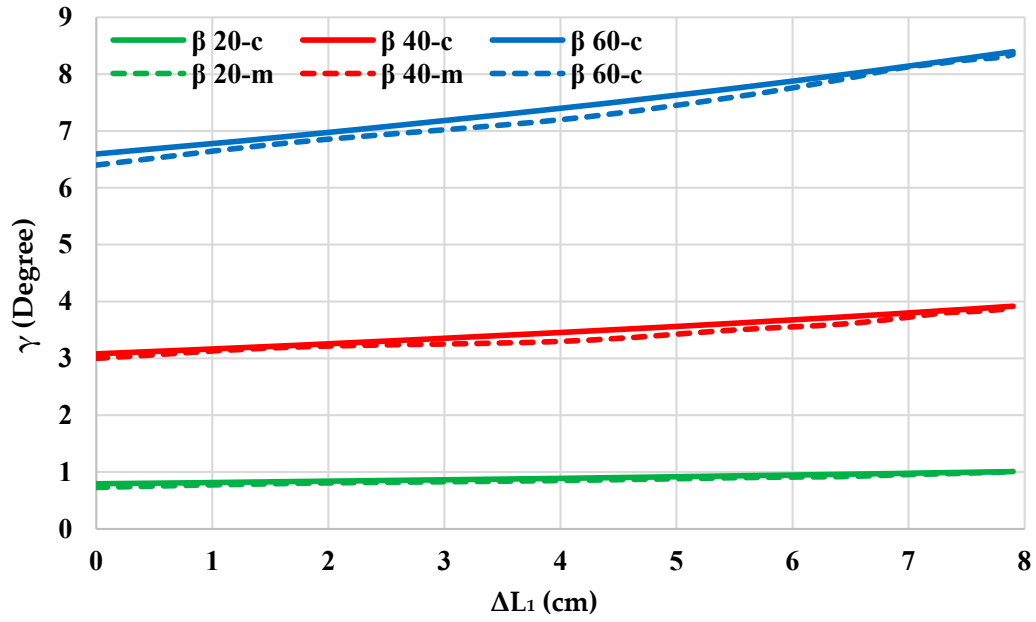

(a)

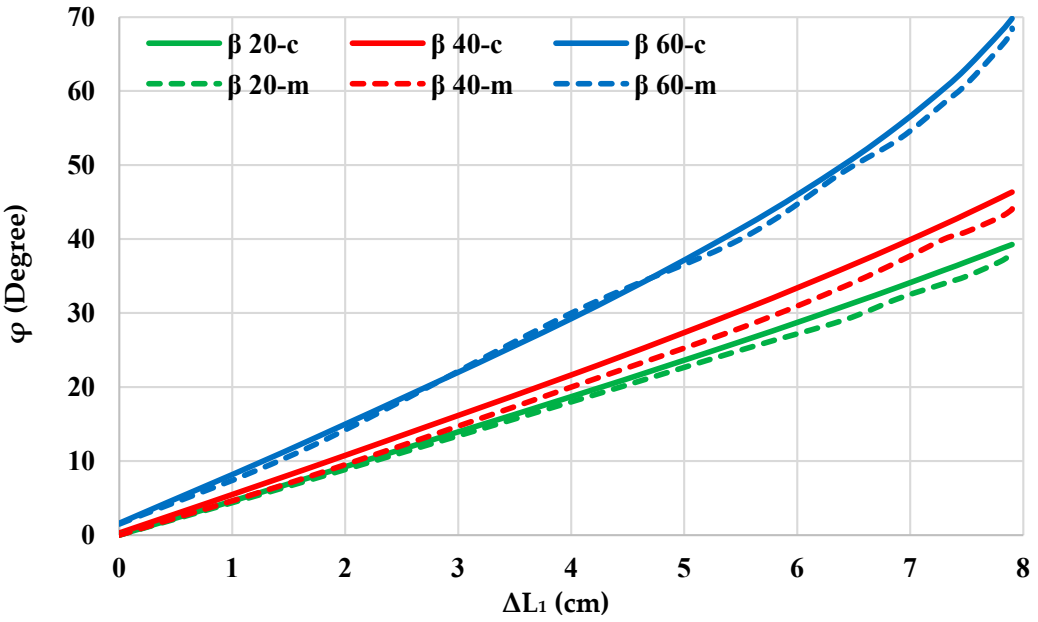

(b)

Figure 9. *Cont.*

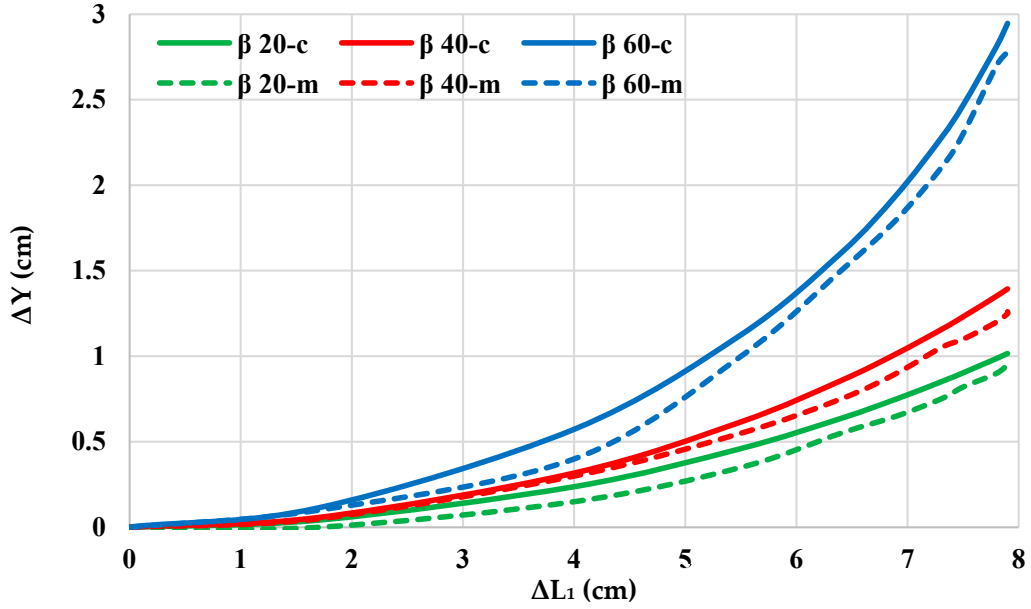

(**c**)

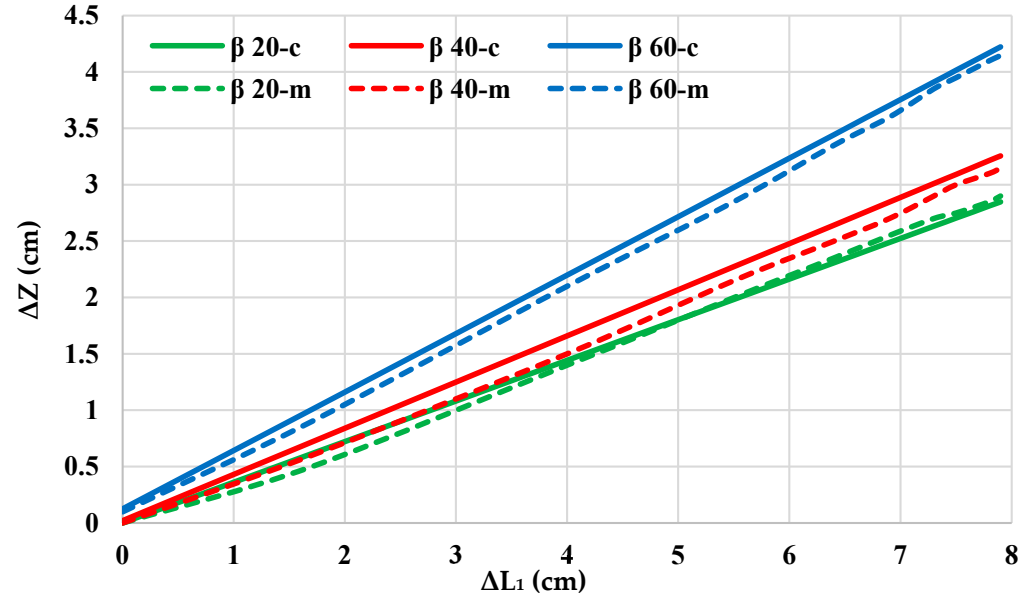

(**d**)

Figure 9. The parameters of the presented soft arm as a function of the left actuator length change at three β values. (**a**) The γ angle. (**b**) The φ angle. (**c**) The position changes in the rotating centre in the Y direction. (**d**) The position changes in the rotating centre in the Z direction.

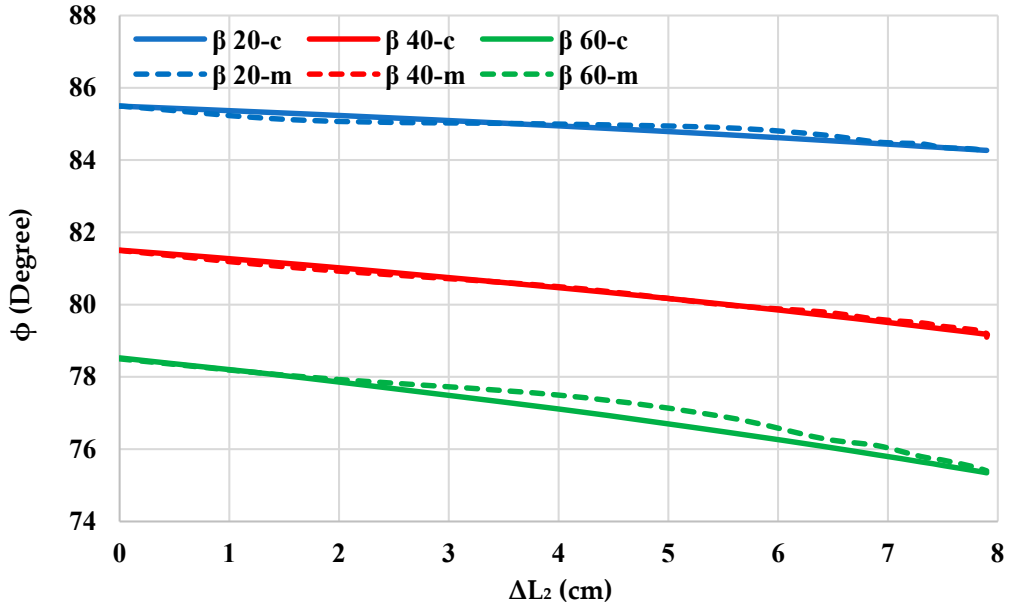

(a)

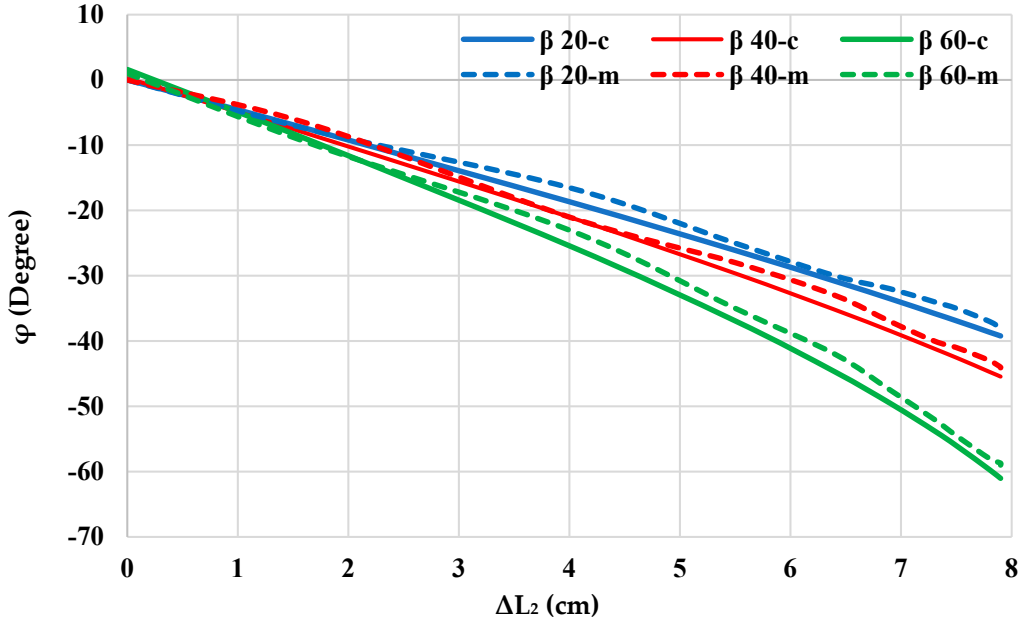

(b)

Figure 10. *Cont.*

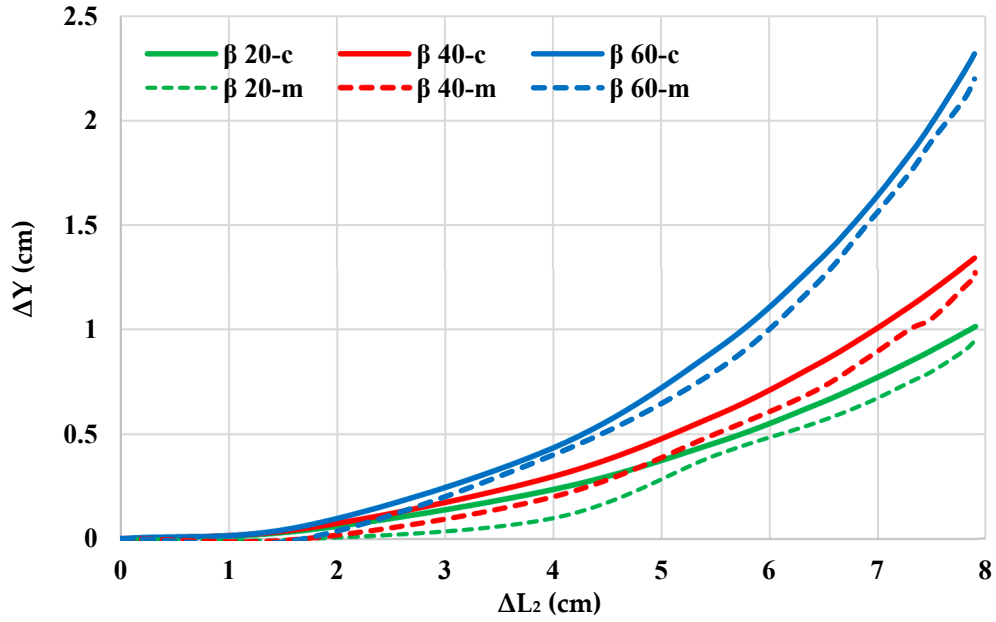

(**c**)

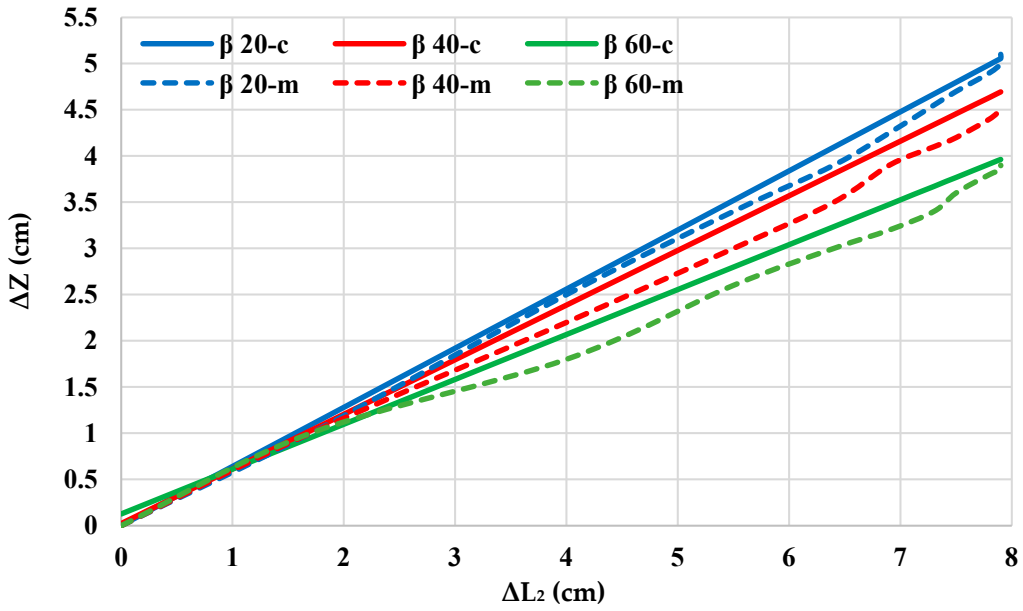

(**d**)

Figure 10. The parameters of the presented soft arm as a function of right actuator length change at three β values. (**a**) The ϕ angle. (**b**) The φ angle. (**c**) The position changes in the rotating centre in the Y direction. (**d**) The position changes in the rotating centre in the Z direction.

Table 3. The validation results due to the variety in both L_1 and L_2.

	Figure 9a–d	**Figure 10a–d**
$R^2(\gamma/\beta = 20/)$	0.99	-
$R^2(\gamma/\beta = 40/)$	0.979	-
$R^2(\gamma/\beta = 60/)$	0.996	-

Table 3. *Cont.*

	Figure 9a–d	Figure 10a–d
$R^2(\varphi/\beta = 20/)$	0.999	-
$R^2(\varphi/\beta = 40/)$	0.997	-
$R^2(\varphi/\beta = 60/)$	0.999	-
$R^2(\Delta Y/\beta = 20/)$	0.981	-
$R^2(\Delta Y/\beta = 40/)$	0.989	-
$R^2(\Delta Y/\beta = 60/)$	0.995	-
$R^2(\Delta Z/\beta = 20/)$	0.996	-
$R^2(\Delta Z/\beta = 40/)$	0.996	-
$R^2(\Delta Z/\beta = 60/)$	0.996	-
$R^2(\phi/\beta = 20/)$	-	0.942
$R^2(\phi/\beta = 40/)$	-	0.994
$R^2(\phi/\beta = 60/)$	-	0.972
$R^2(\varphi/\beta = 20/)$	-	0.997
$R^2(\varphi/\beta = 40/)$	-	0.997
$R^2(\varphi/\beta = 60/)$	-	0.996
$R^2(\Delta Y/\beta = 20/)$	-	0.964
$R^2(\Delta Y/\beta = 40/)$	-	0.984
$R^2(\Delta Y/\beta = 60/)$	-	0.994
$R^2(\Delta Z/\beta = 20/)$	-	0.995
$R^2(\Delta Z/\beta = 40/)$	-	0.997
$R^2(\Delta Z/\beta = 60/)$	-	0.988

Table 4. Load effect on the length and twisting angle.

Load (kg)	Length of the Contraction Actuators (cm)	Twisting Angle (Degree)
0	26	91
0.5	26.3	91
1	26.6	91
1.5	26.75	91
2	26.85	90.9

6. Control the Twisting Angle

The encoder has been used instead of the upper joint in the rotating continuum arm. The encoder sends the rotating angle as feedback, which is proportional to the resistance value to the controller input as shown in Figure 11. The presented controller system, parallel neural network and proportional (PNNP), in the previous article [47] have been used to control the twisting angle. The training process is done by (trainlm) (MATLAB 2020a) for 100 iterations and at 10^{-7} mean square error (MSE).

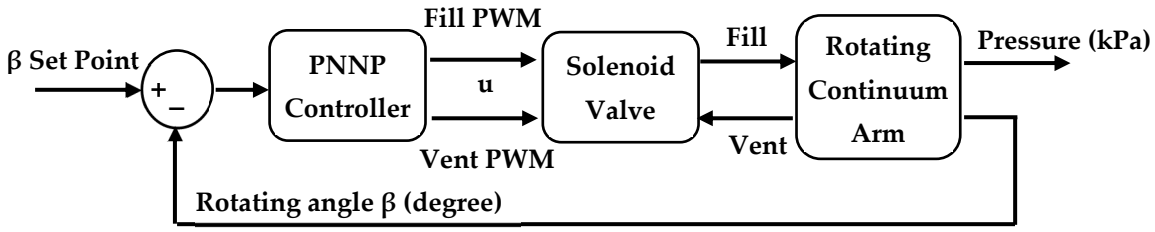

Figure 11. The block diagram of the controller system.

The controller system is built by a parallel structure of the NARMA-L2 Neural Network (NN) control system and proportional (P) controller. The NN ensures accuracy, while the P controller increases the system response [47].

The neural network control system has been trained under the approximation model. The twisting angle of the continuum arm is given by (14) as a function of the duty cycle.

$$y = \frac{90 \times u^*}{98} \tag{14}$$

where y refers to the rotating angle and u^* represents the duty cycle of the pulse width modulation (PWM) signal. The number (90) represents the maximum rotating angle, the 98% is set to be the maximum duty cycle instead of 100% to protect the solenoid valve from the continuous operation. (14) is found by applying different values to the duty cycle for one second and then recording the rotating angle individually by the potentiometer.

The controller outputs for both the neural networks controller and the proportional controller are given below:

The NARMA-L2 NN-controller output $u1$ can be defined as:

$$u1(k) = \frac{y_r(k+1) - f[y_n(k),\ u1_m(k-1)]}{g[y_n(k),\ u1_m(k-1)]} \tag{15}$$

where $f(\ )$ and $g(\ )$ are approximated using neural networks. $y(\ )$ is the system output and:

$$y_n(k) = [y(k),\ \ldots,\ y(k-n+1)]^T \tag{16}$$

$$u1_m(k-1) = [u1(k-1),\ u1(k-2),\ \ldots,\ u1(k-m)]^T \tag{17}$$

where m = 3 and n = 2 and they refer to the 3-delayed plant inputs, and 2-delayed plant outputs, respectively.

On the other hand, the output of the proportional controller is given by:

$$u2(k) = k_p\ \frac{(y_r(k+1) - y(k+1))(u_{max})}{x} \tag{18}$$

x is the maximum rotation angle (90° in this case).

And the overall controlled PWM signal is:

$$u = u1 + u2 \tag{19}$$

Filling and venting the air muscle are two different processes. Therefore, two PNNP controllers are required, one controller for each of them. The control system calculates the error between the reference model (desired rotating angle) and the feedback. Positive error activates the fill controller system, while negative error initiates the vent system. Both branches work together in parallel to gain zero error. Applying sinusoidal validates the controller and rectangular pulse set signals at 0.25 and 0.5 Hz, as shown in Figure 12.

Figure 12 shows the accuracy of the controller system to be used for various rotating angles. The sinusoidal response shows a low constant error because of the small changes in the signal over time.

On the other hand, the rectangular pulse response has a zero steady-state error because of its unchanged values at zero and 75°. The pressure of the two contractors' PMAs does not affect the rotating feature. However, increasing the stiffness of the contraction actuators make them act like bones, similarly, the rectangular pulse response shows that the release time for the SBCA is more than the pressurised period for two reasons: the actuator hysteresis and the pressure difference between the PMA and outside environment. The static and dynamic characteristics of the solenoid valve and the pressure dynamics were ignored in the control process.

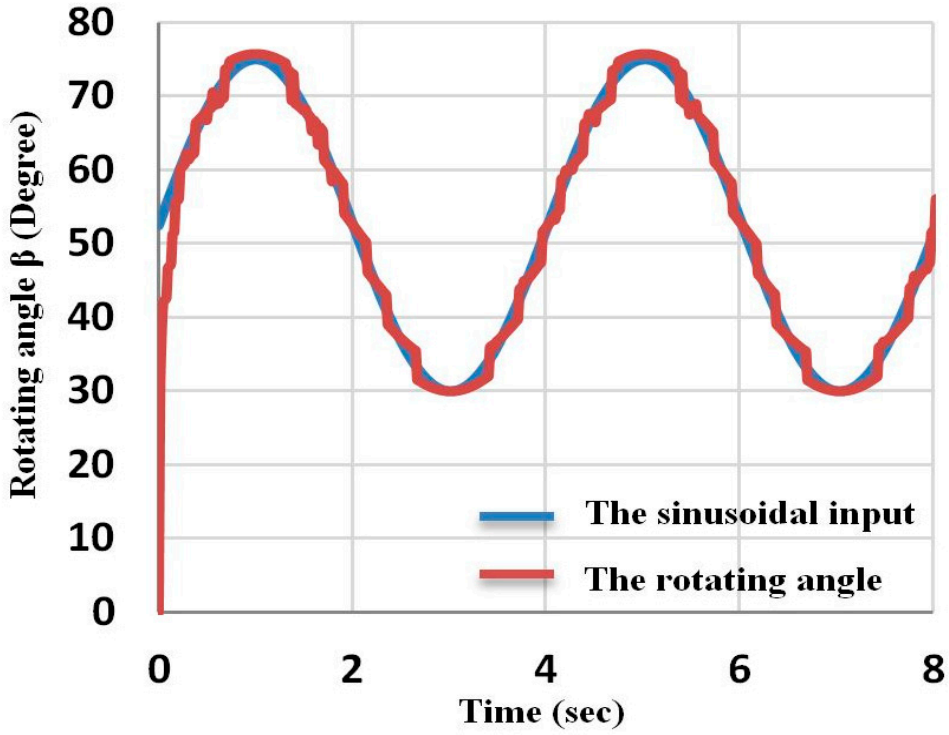

(a)

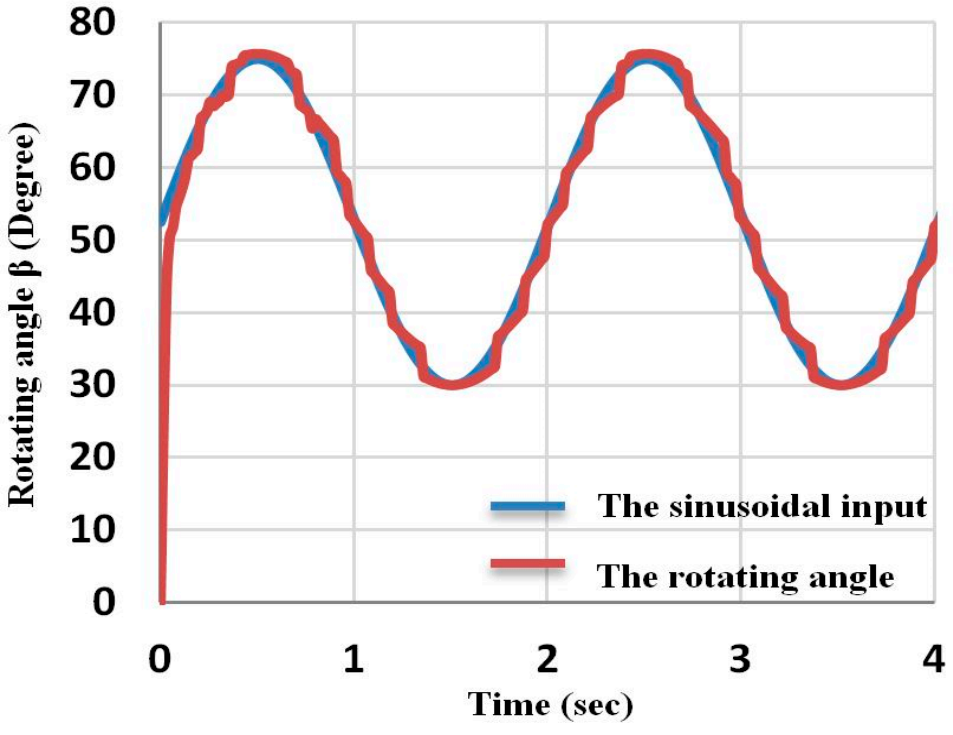

(b)

Figure 12. *Cont.*

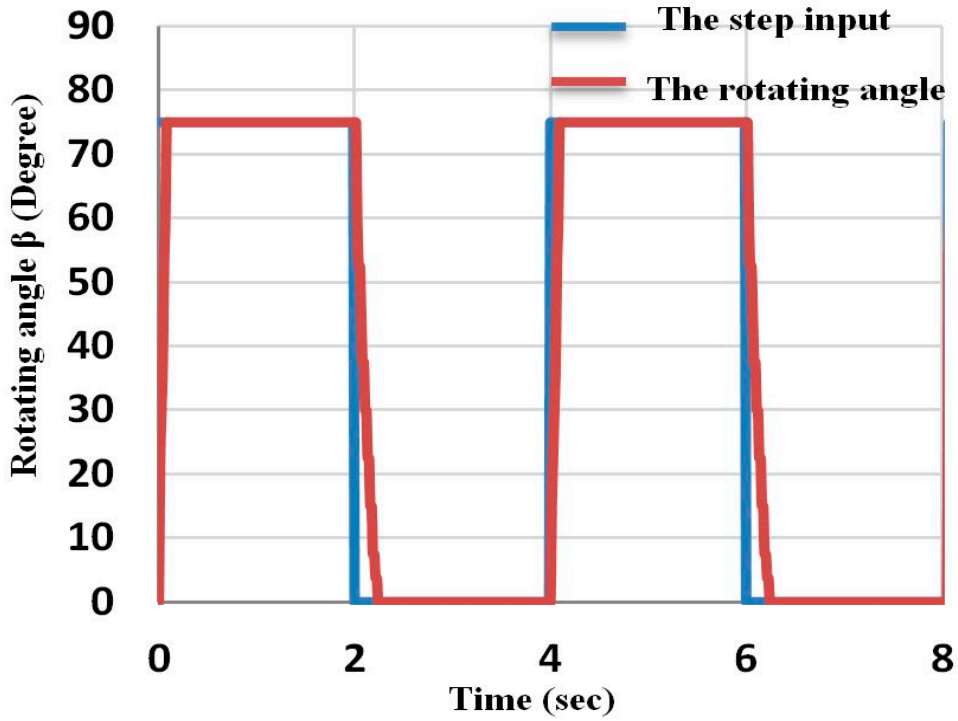

(c)

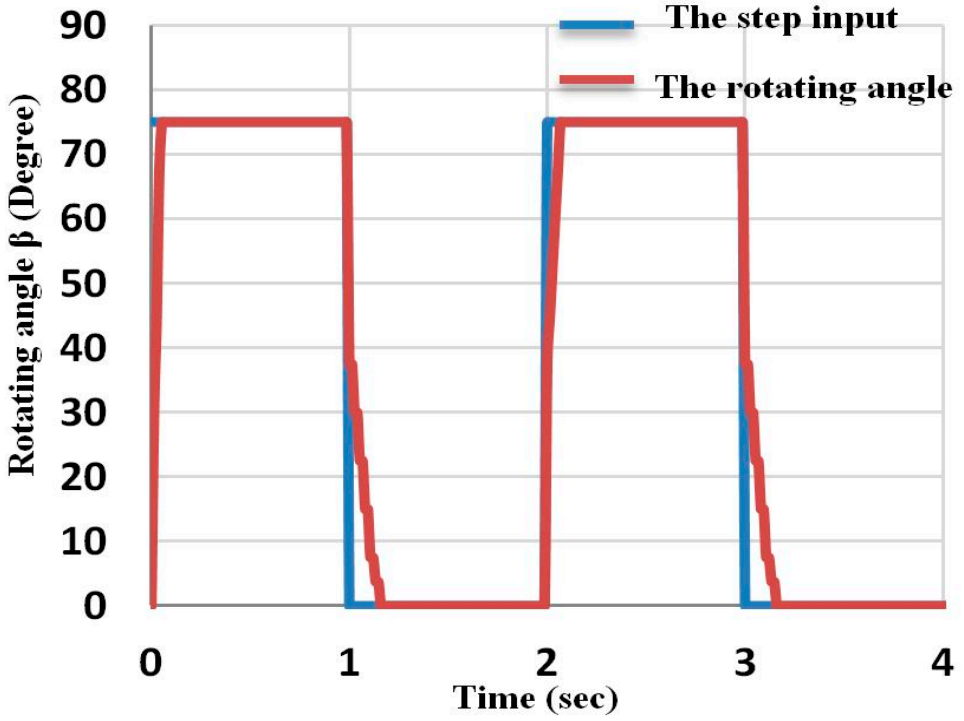

(d)

Figure 12. The controller response for the rotating arm: (**a**) The sinusoidal response at 0.25 Hz, (**b**) The sinusoidal response at 0.5 Hz, (**c**) The rectangular pulse response at 0.25 Hz, and (**d**) The rectangular pulse response at 0.5 Hz.

7. Conclusions

The rotational performance of the individual forearm due to the elbow wrist joints is described briefly in this article. This movement toward clockwise and counterclockwise has been used to design a soft continuum soft robot arm. The major element of the presented robot arm is the pronation and supination performances. In addition to this performance, the suggested continuum robot arm has the ability to bend and contract. These behaviours together with a twisting performance provide a high range of DoF. The novel arm has been constructed by two contraction PMAs in parallel and one SBCA, hence, the kinematics for the rotating behaviour are given under multiple actuation levels for the contraction actuators. To validate the performance of the presented robot arm, a control system is utilised to adjust the twisting angle.

AS illustrated through the article, the presented robot is easy to implement at a low cost, providing a high level of performance in terms of the degree of freedom, force to weight ratio, and robustness.

A potential future work, the presented continuum arm can be used in numerous industrial applications, and the twisting performance might be suitable for disabled people with an unhealthy forearm.

Author Contributions: Formal analysis, K.A.A.; Methodology, A.A.-I., K.A.A., M.A.-A. and H.A.-F.; Project administration, A.A.-I.; Resources, A.A.-I.; Software, K.A.A., M.A.-A. and H.A.-F.; Validation, A.A.-I., K.A.A., M.A.-A. and H.A.-F.; Writing—original draft, A.A.-I.; Writing—review & editing, M.A.-A. All authors have read and agreed to the published version of the manuscript.

Funding: This research received no external funding.

Data Availability Statement: The datasets generated and/or analysed during the current study are available from the corresponding author on reasonable request.

Acknowledgments: Many thanks to the University of Basrah and its computer engineering department to provide the lab facilities.

Conflicts of Interest: The authors declare no conflict of interest.

Nomenclature

ε	The contraction ratio
L_0	The nominal length of the actuator [cm]
L	The length of the actuator [cm]
r_1, r_2	Distance between the rotating centre and contraction PMA [cm]
ΔZ, ΔY	The displacement in both Z and Y directions [cm]
y	The output of the Plant system [Degree]
$u1$	The controller output for the NN controller
k_p	The proportional constant
λ_1	The resultant side distances [cm]
γ	The deviation angle of the left contraction PMA [Degree]
β	The twisting angle [Degree]
φ	The bending angle of the robot arm [Degree]
ϕ	The angle between the second PMA and the vertical layout [Degree]
u^*	The duty cycle of the controlled signal
$u2$	The controller output for the P controller

References

1. Ranjan, R.; Upadhyay, P.K.; Kumar, A.; Dhyani, P. Theoretical and Experimental Modeling of Air Muscle. *J. Emerg. Technol. Adv. Eng.* **2012**, *2*, 112–119.
2. Wickramatunge, K.C.; Leephakpreeda, T. Study on mechanical behaviors of pneumatic artificial muscle. *Int. J. Eng. Sci.* **2010**, *48*, 188–198. [CrossRef]
3. Leephakpreeda, T. Fuzzy logic based PWM control and neural controlled-variable estimation of pneumatic artificial muscle actuators. *Expert Syst. Appl.* **2011**, *38*, 7837–7850. [CrossRef]

4. Jamwal, P.K.; Xie, S.Q. Artificial Neural Network based dynamic modelling of indigenous pneumatic muscle actuators. In Proceedings of the 2012 IEEE/ASME 8th IEEE/ASME International Conference on Mechatronic and Embedded Systems and Applications, Suzhou, China, 8–10 July 2012; pp. 190–195.
5. Kang, B.-S.; Kothera, C.S.; Woods, B.K.S.; Wereley, N.M. Dynamic modeling of Mckibben pneumatic artificial muscles for antagonistic actuation. In Proceedings of the 2009 IEEE International Conference on Robotics and Automation, Kobe, Japan, 12–17 May 2009; pp. 182–187.
6. Trivedi, D.; Rahn, C.D.; Kier, W.M.; Walker, I.D. Soft robotics: Biological inspiration, state of the art, and future research. *Appl. Bionics Biomech.* **2008**, *5*, 99–117. [CrossRef]
7. Godage, I.S.; Walker, I.D. Dual Quaternion based modal kinematics for multisection continuum arms. In Proceedings of the 2015 IEEE International Conference on Robotics and Automation (ICRA), Seattle, WA, USA, 26–30 May 2015; pp. 1416–1422.
8. Zheng, T.; Branson, D.T.; Kang, R.; Cianchetti, M.; Guglielmino, E.; Follador, M.; Medrano-Cerda, G.A.; Godage, I.S.; Caldwell, D.G. Dynamic continuum arm model for use with underwater robotic manipulators inspired by octopus vulgaris. In Proceedings of the 2012 IEEE International Conference on Robotics and Automation, Saint Paul, MN, USA, 14–18 May 2012; pp. 5289–5294.
9. Anh, H.P.H. Online tuning gain scheduling MIMO neural PID control of the 2-axes pneumatic artificial muscle (PAM) robot arm. *Expert Syst. Appl.* **2010**, *37*, 6547–6560. [CrossRef]
10. Thanh, T.D.C.; Ahn, K.K. Nonlinear PID control to improve the control performance of 2 axes pneumatic artificial muscle manipulator using neural network. *Mechatronics* **2006**, *16*, 577–587. [CrossRef]
11. Szepe, T. Accurate force function approximation for pneumatic artificial muscles. In Proceedings of the LINDI 2011—3rd IEEE International Symposium on Logistics and Industrial Informatics, Budapest, Hungary, 25–27 August 2011.
12. More, M.; Liska, O. Comparison of different methods for pneumatic artificial muscle control. In Proceedings of the 2013 IEEE 11th International Symposium on Applied Machine Intelligence and Informatics (SAMI), Herl'any, Slovakia, 31 January–2 February 2013; pp. 117–120.
13. Andrikopoulos, G.; Nikolakopoulos, G.; Manesis, S. Advanced nonlinear PID-based antagonistic control for pneumatic muscle actuators. *IEEE Trans. Ind. Electron.* **2014**, *61*, 6926–6937. [CrossRef]
14. McMahan, W.; Chitrakaran, V.; Csencsits, M.; Dawson, D.; Walker, I.D.; Jones, B.A.; Pritts, M.; Dienno, D.; Grissom, M.; Rahn, C.D. Field trials and testing of the OctArm continuum manipulator. In Proceedings of the Proceedings 2006 IEEE International Conference on Robotics and Automation, 2006. ICRA 2006, Orlando, FL, USA, 15–19 May 2006; pp. 2336–2341.
15. McMahan, W.; Jones, B.A.; Walker, I.D. Design and implementation of a multi-section continuum robot: Air-Octor. In Proceedings of the 2005 IEEE/RSJ International Conference on Intelligent Robots and Systems, Edmonton, AB, Canada, 2–6 August 2005; pp. 2578–2585.
16. Trivedi, D.; Rahn, C.D. Model-Based Shape Estimation for Soft Robotic Manipulators: The Planar Case. *J. Mech. Robot.* **2014**, *6*, 021005. [CrossRef]
17. Neppalli, S.; Jones, B.A. Design, construction, and analysis of a continuum robot. In Proceedings of the 2007 IEEE/RSJ International Conference on Intelligent Robots and Systems, San Diego, CA, USA, 29 October–2 November 2007; pp. 1503–1507.
18. Giannaccini, M.E.; Xiang, C.; Atyabi, A.; Theodoridis, T.; Nefti-Meziani, S.; Davis, S. Novel Design of a Soft Lightweight Pneumatic Continuum Robot Arm with Decoupled Variable Stiffness and Positioning. *Soft Robot.* **2018**, *5*, 54–70. [CrossRef]
19. Al-Ibadi, A.; Nefti-Meziani, S.; Davis, S. Novel models for the extension pneumatic muscle actuator performances. In Proceedings of the 2017 23rd International Conference on Automation and Computing (ICAC), Huddersfield, UK, 7–8 September 2017; pp. 1–6.
20. Al-Ibadi, A.; Nefti-Meziani, S.; Davis, S. The Design, Kinematics and Torque Analysis of the Self-Bending Soft Contraction Actuator. *Actuators* **2020**, *9*, 33. [CrossRef]
21. Sun, J.; Tighe, B.; Liu, Y.; Zhao, J. Twisted-and-Coiled Actuators with Free Strokes Enable Soft Robots with Programmable Motions. *Soft Robot.* **2020**, *8*, 213–225. [CrossRef] [PubMed]
22. Cho, K.H.; Song, M.G.; Jung, H.; Park, J.; Moon, H.; Koo, J.C.; Nam, J.-D.; Choi, H.R. A robotic finger driven by twisted and coiled polymer actuator. In Proceedings of the Electroactive Polymer Actuators and Devices (EAPAD) 2016, Las Vegas, NV, USA, 20–24 March 2016.
23. Liu, T.; Wang, Y.; Lee, K. Three-Dimensional Printable Origami Twisted Tower: Design, Fabrication, and Robot Embodiment. *IEEE Robot. Autom. Lett.* **2018**, *3*, 116–123. [CrossRef]
24. Helps, T.; Taghavi, M.; Wang, S.; Rossiter, J. Twisted Rubber Variable-Stiffness Artificial Muscles. *Soft Robot.* **2020**, *7*, 386–395. [CrossRef] [PubMed]
25. Shintake, J.; Cacucciolo, V.; Floreano, D.; Shea, H. Soft Robotic Grippers. *Adv. Mater.* **2018**, *30*, 1707035. [CrossRef] [PubMed]
26. Farrow, N.; Correll, N. A soft pneumatic actuator that can sense grasp and touch. In Proceedings of the IEEE International Conference on Intelligent Robots and Systems, Hamburg, Germany, 28 September–2 October 2015.
27. Yap, H.K.; Ng, H.Y.; Yeow, C.H. High-Force Soft Printable Pneumatics for Soft Robotic Applications. *Soft Robot.* **2016**, *3*, 144–158. [CrossRef]
28. Jackson, N.; Chastain, P.; Crowther, M.; Shin, M. Development of Fast Prototyping Pneumatic Actuated Grippers. *Int. J. Precis. Eng. Manuf.* **2019**, *20*, 2183–2192. [CrossRef]
29. Schmitt, F.; Piccin, O.; Barbé, L.; Bayle, B. Soft Robots Manufacturing: A Review. *Front. Robot. AI* **2018**, *5*, 84. [CrossRef]

30. Robinson, G.; Davies, J.B.C. Continuum robots—A state of the art. In Proceedings of the 1999 IEEE International Conference on Robotics and Automation (Cat. No.99CH36288C), Detroit, MI, USA, 10–15 May 1999; Volume 4, pp. 2849–2854.
31. Gong, Z.; Chen, B.; Liu, J.; Fang, X.; Liu, Z.; Wang, T.; Wen, L. An Opposite-Bending-and-Extension Soft Robotic Manipulator for Delicate Grasping in Shallow Water. *Front. Robot. AI* **2019**, *6*, 26. [CrossRef]
32. Shih, B.; Christianson, C.; Gillespie, K.; Lee, S.; Mayeda, J.; Huo, Z.; Tolley, M.T. Design considerations for 3D printed, soft, multimaterial resistive sensors for soft robotics. *Front. Robot. AI* **2019**, *6*, 30. [CrossRef]
33. Cullinan, M.F.; Bourke, E.; Kelly, K.; McGinn, C. A McKibben Type Sleeve Pneumatic Muscle and Integrated Mechanism for Improved Stroke Length. *J. Mech. Robot.* **2017**, *9*, 011013. [CrossRef]
34. Al-Ibadi, A.; Nefti-Meziani, S.; Davis, S. A circular pneumatic muscle actuator (CPMA) inspired by human skeletal muscles. In Proceedings of the 2018 IEEE International Conference on Soft Robotics (RoboSoft), Livorno, Italy, 24–28 April 2018; pp. 7–12.
35. Satheeshbabu, S.; Krishnan, G. Modeling the Bending Behavior of Fiber-Reinforced Pneumatic Actuators Using a Pseudo-Rigid-Body Model. *J. Mech. Robot.* **2019**, *11*, 031011. [CrossRef]
36. Haddadin, S.; Albu-Schaffer, A.; Hirzinger, G. Dummy Crashtests for Evaluation of Rigid Human-Robot Impacts. Available online: https://citeseerx.ist.psu.edu/viewdoc/download?doi=10.1.1.525.296&rep=rep1&type=pdf (accessed on 6 April 2022).
37. Szalai, S.; Dogossy, G. Speckle pattern optimization for DIC technologies. *Acta Tech. Jaurinensis* **2021**, *14*, 228–243. [CrossRef]
38. Dobra, P.; Jósvai, J. OEE measurement at the automotive semi-automatic assembly lines. *Acta Tech. Jaurinensis* **2021**, *14*, 24–35. [CrossRef]
39. Kozakiewicz, B.; Warsaw, T.W. Spring Based on Flat Permanent Magnets: Design, Analysis and Use in Variable Stiffness Actuator. Available online: http://casopisi.junis.ni.ac.rs/index.php/FUMechEng/article/view/6852 (accessed on 6 April 2022).
40. Vanderborght, B.; Albu-Schaeffer, A.; Bicchi, A.; Burdet, E.; Caldwell, D.G.; Carloni, R.; Catalano, M.; Eiberger, O.; Friedl, W.; Ganesh, G.; et al. Variable impedance actuators: A review. *Rob. Auton. Syst.* **2013**, *61*, 1601–1614. [CrossRef]
41. Fryman, J.; Matthias, B. Safety of industrial robots: From conventional to collaborative applications. In Proceedings of the 7th German Conference on Robotics, Munich, Germany, 21–22 May 2012; pp. 51–55.
42. Youm, Y.; Dryer, R.F.; Thambyrajah, K.; Flatt, A.E.; Sprague, B.L. Biomechanical analyses of forearm pronation-supination and elbow flexion-extension. *J. Biomech.* **1979**, *12*, 245–255. [CrossRef]
43. James, B. Pianism: Performance communication and the playing technique. *Front. Psychol.* **2018**, *2018*, 2125. [CrossRef]
44. Hamill, J.; Knutzen, K.M.; Derrick, T.R. *Biomechanical Basis of Human Movement*, 4th ed.; Wolters Kluwer Health Adis (ESP): London, UK, 2014; ISBN 9781469891828.
45. Mukhopadhyay, P.; O'Sullivan, L.; Gallwey, T.J. Estimating upper limb discomfort level due to intermittent isometric pronation torque with various combinations of elbow angles, forearm rotation angles, force and frequency with upper arm at 90° abduction. *Int. J. Ind. Ergon.* **2007**, *37*, 313–325. [CrossRef]
46. Al-Ibadi, A.; Nefti-Meziani, S.; Davis, S. Valuable experimental model of contraction pneumatic muscle actuator. In Proceedings of the 2016 21st International Conference on Methods and Models in Automation and Robotics (MMAR), Miedzyzdroje, Poland, 29 August–1 September 2016; pp. 744–749.
47. Al-Ibadi, A.; Nefti-Meziani, S.; Davis, S. Controlling of Pneumatic Muscle Actuator Systems by Parallel Structure of Neural Network and Proportional Controllers (PNNP). *Front. Robot. AI* **2020**, *7*, 115. [CrossRef]